Hashim Jabbar [1*]
Maan Al-Nuaim [2]
Sumaia H. Gatia [1]
Anwar A. Jumaa [3]
Zuhair Ali Abdulnabi [3]

[1] Department of Physics, College of Science, University of Basrah, Basrah, IRAQ
[2] Department of Pharmaceutical Chemistry, College of Pharmacy, University of Basrah Basrah, IRAQ
[3] Department of Marine Chemistry, Marine Science Center, University of Basrah,-Iraq Basrah, IRAQ

** For supplementary materials, the corresponding author (H. Jabbar) can be contacted at hashim.jabbar@uobasrah.edu.iq*

Concentration Dependence of Magnetothermal Response in Fe_3O_4 Nanofluid

In this study, magnetite magnetic nanoparticles (MNPs) were investigated in both low and high concentration ranges to evaluate and optimize the heating efficiency. The Fourier-transform infrared (FTIR) spectroscopy confirmed pure Fe_3O_4 nanoparticles and the x-ray diffraction (XRD) pattern indicated their inverse spinel structure. The mean particle size was calculated using a scanning electron microscopy (SEM) and the hydrodynamic size was determined using dynamic light scattering (DLS). Dipolar interactions that might influence magnetic hyperthermia (MHT) were found by the quantitative study of M-H loops of Fe_3O_4 nanoparticles and analyzed with first order reversal curves (FORC) using a vibrating sample magnetometer (VSM). Calorimetric results exhibited SLP concentration-dependent oscillation behavior. These results of magnetic and calorimetric measurements on Fe_3O_4 nanoparticles and their fluids might be useful to identify the key elements that contribute finding best heating efficiency with lower dosage and consequent toxicity which represents a challenge in using Fe_3O_4 nanoparticles for MHT.

***Keywords*:** Magnetite; Nanoparticles; Co-precipitation; Superparamagnetic
Received: 2 January 2025; **Revised:** 19 May 2025; **Accepted:** 26 May 2025

1. Introduction

Magnetic fluid hyperthermia (MFH) is noninvasive, has the potential to treat specific types of cancer locally, and has no therapeutic upper limit. Due to this facts, MFH has garnered interest as a cancer therapy, in which magnetic nanoparticles are used as heat mediators [1-5]. When an external alternating magnetic field is applied to the magnetic fluid (MF), the magnetic vector M in the sample reorients in space in the direction of the magnetic field intensity vector H. A portion of the magnetic field energy is irreversibly converted into thermal energy as a result of the phase delay between the magnetic vector M and the vector H. As a result, heat is produced in the MF sample, which can be used in biomedicine to eradicate cancer cells [6].

The medical use of biocompatible magnetic fluids is significant in treating "hyperthermia," a condition where particular body organs or tissues are heated to temperatures between 41 and 46 °C. It is possible to modify the heat generating capability of iron oxide, the most popular heat generator platform, by doping with other metals or altering the size or shape. For example, dopants such as Co, Mn, or Zn can be added to regulate the magnetic anisotropy, which might enhance heat induction [7-10]. The Food and Drug Administration (FDA) has only approved pure iron oxide as an inorganic material; ferrite materials that contain doped metals need to have their biocompatibility confirmed before being used in clinical settings. Thus, it is justified to develop iron oxide nanoparticles with high heat generation efficiencies for clinical application, particularly in the treatment of cancer.

Realizing the perfect parameter combinations for magnetic nanoparticles (MNPs) and applied fields is one of the primary challenges nowadays to optimize the heat induction efficiency [11]. The wide range of parameters makes trial-and-error methods notoriously challenging. Consequently, it would be ideal to have a deeper comprehension of the physical mechanism that underlies the heat induction. While earlier studies focused on magnetic losses of individual MNPs, many recent works consider also the effect of interactions and MNPs concentration on heating efficiency. The latter is commonly expressed in terms of the specific loss power (SLP), also known as the specific absorption rate, which is the volumetric work performed by the magnetic mass density and the external field per unit cycle [12,13]. The concentration-dependence of the SLP is currently a topic of debate in the literature. SLP decreased as the MNP concentration increased, according to several experimental investigations. Kim et al. [14] recently confirmed the non-monotonic behavior of SLP with concentration, which Martinez-Boubeta et al. had previously reported [15]. This would imply that there may be ideal MNPs concentration conditions for MFH

that optimize heating efficiency [16]. Some studies suggest that dipolar interactions, inherent properties of MNPs and cluster morphologies, or Brownian rotating particle motion may be responsible for the disparities in results [17-19]. Other relevant theoretical studies obtain various conclusions, some of these recommendations seem to be supported by a recent simulation research that found chain-formation to improve SLP [20].

The aim of this study is to produce Fe_3O_4 nanoparticles system with effective hyperthermia characteristics utilizing easy, one-pot synthetic methods and cheap precursors. The synthesis procedure may also be carried out in an air environment without the need of sophisticated devices. In order to investigate the impact of Fe_3O_4 nanoparticles concentration on hyperthermia, the aim includes synthesizing pure Fe_3O_4 nanoparticles with a moderate magnetization and studying the structural, compositional, morphological, and relevant magnetic properties of single Fe_3O_4 nanoparticles system.

2. Experimental Procedures

Ammonium hydroxide (NH_4OH), 32% ammonia in water, ferric chloride hexahydrate ($FeCl_3.6H_2O$) and ferrous chloride hexahydrate ($FeCl_2.6H_2O$), ethanol (C_2H_5OH), and the cleaning solution provided by Merck, Bendosen Germany, and R&M companies, respectively, were used to synthesize Fe_3O_4 nanoparticles.

The following procedure was used to produce the magnetite nanoparticles. A 10.33 mL of double-distilled water was mixed with 3 mL of $FeCl_3$, 2 mL of $FeCl_2$ (2 mol L^{-1} dissolved in 20 mol L^{-1} dionized water (DI) water). Then 2 mL of NaOH (5 mol L^{-1}) was added to the former solution dropwise over the course of one minute while being magnetically stirred. Shortly after the solutions were combined, the color of the solutions changed from pale yellow to red, signifying the formation of complex ions between the Fe^{3+} and NaOH. A 200 mL of DI water were added to the solution after it had been rapidly stirred until its color restored. Under magnetic stirring, a black precipitate rapidly developed and was left to crystallize fully for an additional half hour. The precipitate was separated by magnetic decantation and repeatedly washed with DI water until the pH of the suspension reached 7.5. The suspension was finally vacuum-dried to a black powder at ambient temperature.

After the Fe_3O_4 nanoparticles samples were synthesized, their crystalline structure and crystallite size were investigated using X-ray diffraction (XRD; Philips, model X'Pert Pro; Cu Kα radiation with (λ = 0.154 nm). In addition, energy dispersive spectroscopy (EDS) for elemental analysis, mean NP diameter, and particle shape were obtained using field-emission scanning electron microscopy (FE-SEM; MIRA3 TESCAN). Finely ground samples were dispersed throughout KBr pellets, and FTIR spectra were recorded using a Spectrum BX spectrometer (Perkin Elmer) in transmission mode with a resolution of 4 cm^{-1}. We used dynamic light scattering (DLS) to determine the size distribution of the particles in the suspension or aqueous solution. Hysteresis loops were measured using a vibrating sample magnetometer (VSM; MDK, University of Basrah) to investigate the magnetic properties at room temperature. To evaluate the hysteresis loop results and provide more details on the magnetic characteristics of Fe_3O_4 nanoparticles, a FORC analysis was also performed. The FORC analysis was conducted using the following procedure: The sample was first subjected to a magnetic field that was positively saturated (H_{max}). The initial reversal curve of the NP sample was then created by sweeping this field back to H_{max} Using specific steps, this field was reduced to a reversal field H_r ($H_r<H_{max}$). (Hyperthermia; MDK, University of Basrah) have been utilized to gather data of calorimetric measurements of hyperthermia application.

3. Results and Discussion

XRD provided confirmation of the iron oxide phase, magnetite, that was expected to form under the synthetic conditions used [21,22]. As depicted in Fig. (1), the peaks were consistent and easily indexed as an inverse cubic spinal structure of pure Fe_3O_4 phase. In conjunction with the XRD pattern analysis, inverse cubic spinel structure of Fe_2O_3 nanoparticles was identified by the JCPDS card no. 01-075-0033 (see lower panel of Fig. 1) [2]. Using the Scherer equation, the mean particle diameters were also computed from the XRD pattern based on the line width of the (311) plane refraction peak [22]

$$D = \frac{k\lambda}{\beta \cos\theta} \quad (1)$$

The reference peak width at angle θ is being used in the equation, where λ is the X-ray wavelength (1.5418 Å), β is the full-width at half maximum (FWHM), and k is a shape factor that is approximately 0.9 for magnetite [22]. The analyses for magnetite nanoparticles were 7.46 nm.

Table (1) The computed distance of crystalline lattice planes (d-spacing) determined from XRD analysis and calculated theoretical data of reference card (d-value) for pure Fe_3O_4 NPs

2θ (deg)	(hkl)	d-spacing [XRD] (Å)	d-value [Ref. card] (Å)
30.4198	(220)	2.94869	2.938
35.7768	(311)	2.50898	2.508
43.4064	(400)	2.07924	2.077
53.7803	(422)	1.70643	1.696
57.3885	(511)	1.60339	1.599

FTIR is an absorption-based technique that measures the energy of molecular vibrations after a sample is subjected to infrared light. The distinctive bands of the spectra are used to identify the chemical

fingerprint of Fe_3O_4 MNPs. The transmitted radiation is detected, while the remainder is absorbed in the sample. Figure (2) displays the FTIR spectrum derived from pure magnetite nanoparticles. The stretching vibration mode linked to the metal-oxygen Fe-O bond in the crystalline lattice of Fe_3O_4 is responsible for the strong peak observed at 553.3 cm^{-1}. Ferrites in particular and all spinel structures in general have similar peak prominently [23-25]. The presence of hydroxyl groups is associated with a band centered at 1637 cm^{-1} and a broad band centered at 3368 cm^{-1} which are ascribed to OH-bending and OH- stretching, respectively.

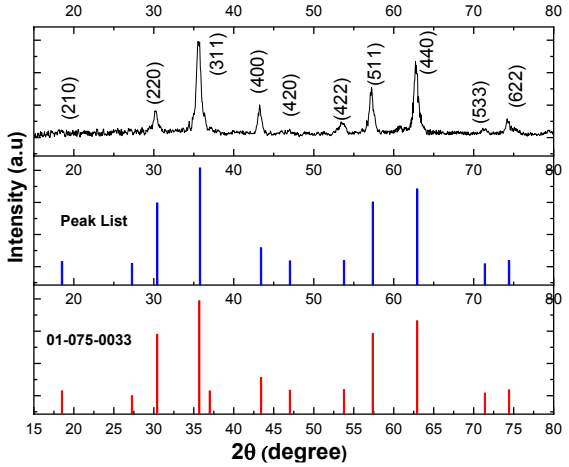

Fig. (1) XRD patterns of the Fe_3O_4 NPs (top), peaks list (middle) the JCPDS reference card (bottom)

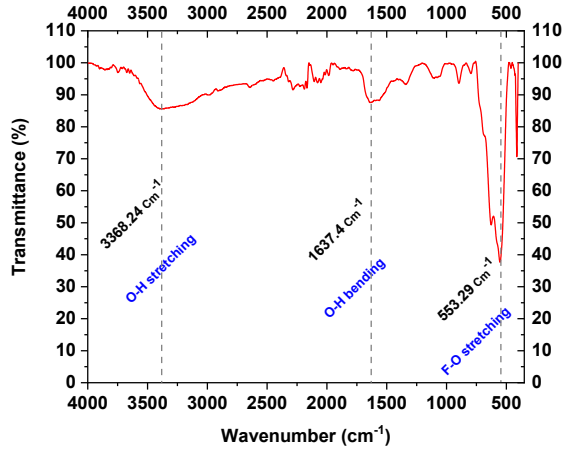

Fig. (2) FTIR spectrum showing stretching and bending vibrations of the synthesized pure Fe_3O_4 MNPs

Figure (3) displays the co-precipitated Fe_3O_4 NPs, corresponding particle diameter distribution histograms, and EDS spectra obtained with a FESEM. It is possible to recognize a nearly spherical shape of the Fe_3O_4 nanoparticles in this image. The expected significant distribution histograms of Fe_3O_4 nanoparticles and the mean diameter is also shown. The mean diameter value ~42 nm, by which we can conclude there is a large difference between $d_{(XRD)}$ and $d_{(FESEM)}$, as determined by the XRD and FE-SEM analyses, respectively, the agglomeration of Fe_3O_4 nanoparticles might be significant. The polycrystalline nature of the Fe_3O_4 nanoparticles is suggested by the fact that $d_{(XRD)}$ is smaller than $d_{(FESEM)}$. On the other hand, the size distribution of the nanoparticles might result from the absence of surfactant after the synthesis process [26]. With a mean of 42 nm and a standard deviation of 2.22 nm, the nanoparticles show a size distribution that is well fitted by a log-normal distribution function. They are highly uniform in size and have a quasi-spherical shape. This is well demonstrated by the histogram in Fig. (3b), which was created by statistically analyzing SEM images of the Fe_3O_4 nanoparticles using ImageJ software. SEM images also reveal some aggregation state. Strong dipole-to-dipole magnetic interactions may be the cause of the aggregates of uncoated Fe_3O_4 nanoparticles. EDX is a method used for determining the composition and structure of Fe_3O_4 magnetic nanoparticles and to analyze the samples at a 15 kV acceleration voltage. Figure (3c) shows EDX spectrum of the synthesized Fe_3O_4 nanoparticles. The peaks at 0.9, 6.1, and 7 keV are linked to the binding energies of iron, along with the oxygen peak at 0.5 keV. Consequently, the EDX confirmed that nanoparticles were iron and oxygen. The atomic percentages for O and Fe, as determined by EDX quantification, were 37.53% and 62.47%, respectively. In summary, the purity of nanoparticles was proved due to the absence of carbon or other elements detected by the sample EDX spectrum.

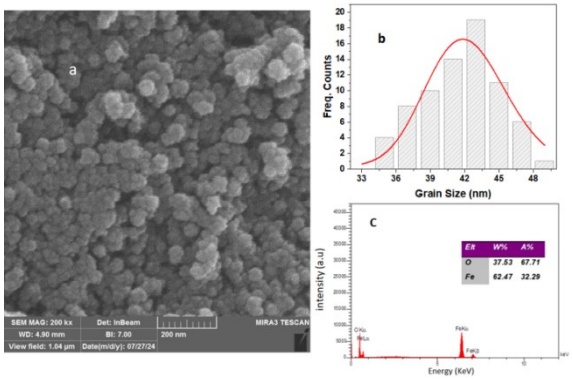

Fig. (3) FE-SEM micrograph (a), grain size distribution histograms based on the FE-SEM images (b) and EDS spectrum (c) of Fe_3O_4 MNPs sample. The corresponding elemental analysis is presented in the insets of EDS spectrum

An established method for determining the average size and size distribution of particles in a suspension is dynamic light scattering, or DLS. Compared to electron microscopy, the method has the advantages of being noninvasive, comparatively quick, and requiring less sample preparation. In just a few minutes, the noninvasive experiment can reveal details about the size and homogeneity of biomolecules using just 12 µL of sample. It is possible to track sample properties

such as aggregation, folding, or conformation in relation to different preparations, solvent conditions, temperature, or time. The polydispersity index (PDI), an output of the autocorrelation function, shows the range of particle sizes. PDI values range from 0 to 1, where 0 represents a highly homogeneous population of nanoparticles and 1 represents a highly heterogeneous population.

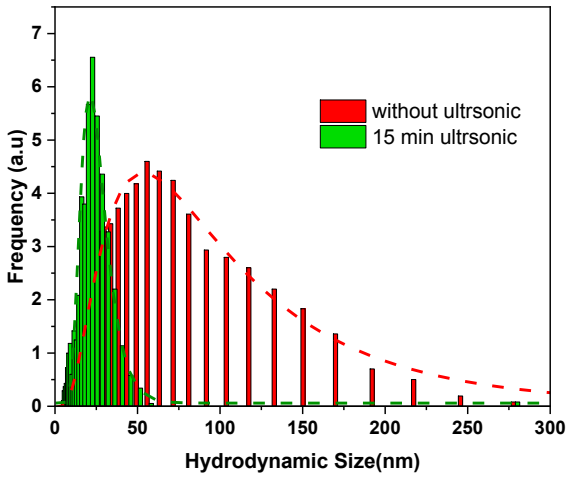

Fig. (4) DLS particle hydrodynamic size distribution statistical histograms for Fe_3O_4 NPs with (green) and without (red) ultrasonic (the dashed lines shows the distributions of the samples with and without ultrasonic exposure fitted using the LogNormal function)

With this technique, nonspherical particles, such as rods, may also be analyzed using multiangle DLS. [27,28]. The stability of MNPs in solution was evaluated as a critical component for their potential use in biomedical applications. The hydrodynamic size distributions derived from the DLS analysis are shown in Fig. (4). The aggregate sizes obtained from the FE-SEM scanning are substantially smaller, with a PDI of around 0.482, than the DLS hydrodynamic sizes, which are roughly 121 nm without ultra-sonication. Nevertheless, during 15 minutes of ultra-sonication, the hydrodynamic mean size of MNPs aggregates drops to 26 nm, with a PDI of 0.168 nanoparticles aggregates.

The M-H loops of NP sample were initially measured at room temperature with a maximum applied magnetic field of 5 kOe. Figure (5) shows pure Fe_3O_4 nanoparticles hysteresis loops. The quantitative results from the hysteresis loop measurements for saturation magnetization (Ms), remanence magnetization (Mr), and coercivity (Hc) were calculated. It is evident that the sample Ms values are 38.73, and its Hc is 3.1 Oe. The maximum Ms of bulk Fe_3O_4 material, which is roughly 90 emu/g is greater than this value [29]. One crucial factor in the conception of magnetic nanoparticle systems for hyperthermia that are optimized for particular magnetic field amplitudes is the control of the magnetic anisotropy through interactions and crystallinity. For instance, a lower anisotropy (lower Hc) is necessary for low field applications [30].

A closer look at the magnetic properties was also made possible by the use of FORC analysis to evaluate the hysteresis loop results. In fact, FORC measurements capture the magnetic fingerprints of materials and reveal the distributions of coercive and interaction fields [31,32]. After being ground into a powder, the samples used for the FORC measurements were firmly compressed into gel caps to immobilize them. A Vibrating Sample Magnetometer (VSM; MDK) was used to perform FORCs at room temperature. For each FORC measurement, the sample is saturated with a positive applied field of 1 T before tracing 50 magnetization curves M(Hr,H) at a reversal field Hr from the major hysteresis loop M(H), with H acting as the measurement point along the loop. The average measurement time was 100 ms, and the field increment was 2.3 mT. The FORC distribution is obtained by a mixed second-order derivation as follows:

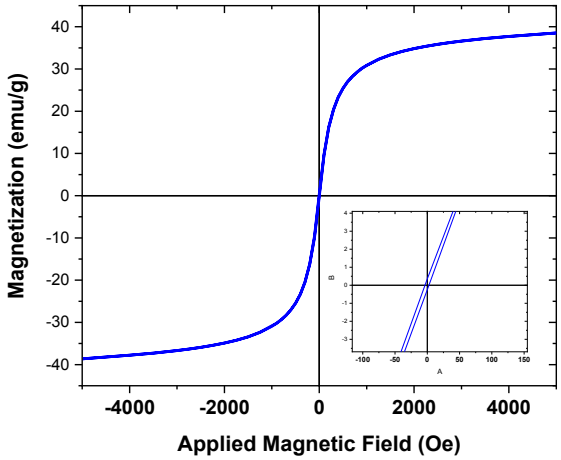

Fig. (5) Room-temperature M-H loops of a pure Fe_3O_4 MNPs sample. The hysteresis loop magnified at a lower magnetic field range in the bottom-right inset

A set of FORC is used to compose a detailed FORC diagram as shown in Fig. (6a). The saturation of a system in a positive applied field comes before the creation of a FORC. A FORC is the magnetization curve that emerges when the applied field is raised back to saturation after the field has been reduced to a reversal field Hr. M(Hr,H) represents the magnetization at the applied field H on the FORC with reversal field Hr [33]. The mixed second derivative is the definition of the FORC distribution:

$$\rho(H, H_r) = -\frac{1}{2}\frac{\partial^2 M(H,H_r)}{\partial H \partial H_r} \qquad (2)$$

We use FORC datasets, which have both the applied and reversal fields with a uniform field spacing H_{Sp}. We use a polynomial fit on a local neighborhood made up of a square with five data

points on each side to calculate the second derivative in Eq. (2) on a dataset, where *Hc* and *Hu* axes are defined by the equations:

$$H_C = \frac{H-H_r}{2}, H_u = \frac{H+H_r}{2} \quad (3)$$

The coordinate system can be altered from (H,Hr) to (Hc,Hu), where Hc represents for the coercive force and Hu for the interaction field. A FORC diagram is a contour plot of the FORC distribution with H_u on the vertical axes and Hc on the horizontal (see Fig. 6a). All FORC diagrams are processed using a smoothing factor (S.F.) of two. The horizontal axis of the FORC diagram, which represents the coercive field (Hc), is sensitive to grain size and composition, whereas the vertical axis (Hu) displays information on the magnetic interaction between particles.

Reversible and irreversible magnetizations combine to form a magnetic response of material. A FORC distribution, it has been demonstrated that extended FORCs can capture a reversible magnetization. The definition of an extended FORC is:

$$M(H_r, H) \equiv \begin{cases} M(H_r, H) \text{ if } H \geq H_r \\ M(H_r, H_r) \text{ if } H < H_r \end{cases} \quad (4)$$

The reversible ridge on the Hc=0 axis that results from calculating the FORC distribution using the extended FORCs in Eq. (4) is given by:

$$\rho(H_C = 0, H_u) = \frac{1}{2}\delta(H_C) lim_{H \to H_r} \frac{\partial^2 M(H,H_r)}{\partial H \partial H_r}\Big|_{H_r = H_C} \quad (5)$$

The slope of the FORC with reversal field Hr=Hu, when that FORC is connected to the primary hysteresis loop, is the derivative in Eq. (5). At applied field Hu, this is comparable to the reversible susceptibility on the descending main hysteresis loop. The full magnetic response is captured by the FORC distribution with the expanded FORCs in Eq. (4), ensuring that the total weight distribution equals the saturation magnetization [34,35].

In the case that a system has a reversible magnetization of the simple form M_{rev} (H), the FORC distribution of the form will exhibit a delta function ridge.

$$\rho(H_C, H_u) = \frac{1}{2}\delta(H_C)\frac{dM_{rev}(H_u)}{dH_u} \quad (6)$$

In a broader sense, the irreversible and reversible magnetizations will be connected. The "reversible magnetization" might not be universally reversible, according to this connection. Therefore, characteristics outside the Hc=0 axis that are part of the FORC distribution may really be contributed by the "reversible magnetization" as shown in Fig. (6b) and Fig. (6c).

This particulate system can be approximately described as a collection of square hysterons if temperature and interaction effects are disregarded. We would anticipate that the FORC distribution caused by the square hysterons in this straightforward approach would have a steeply peaked horizontal crest on the Hu=0 axis. Experimental evidence has demonstrated that this spread grows as particle concentration rises. This implies that dipole interactions are mostly responsible for the bias distribution spread, and that the degree of spread can be used to gauge the intensity of the interaction when analyzing nanoparticle systems. The SP fraction of the sample 46.16% which was calculated using M-H loops.

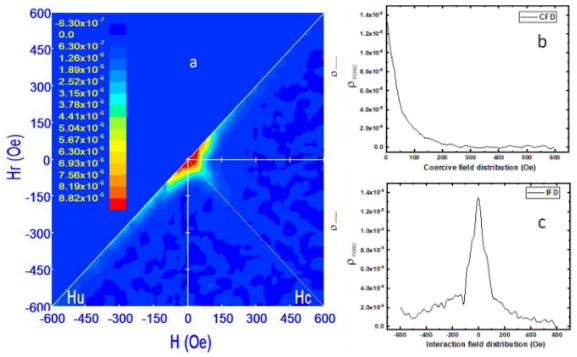

Fig. (6) (a) Room-temperature measurements of Fe_3O_4 NPs two-dimensional FORC diagrams. The distribution of the NPs system coercive and interaction fields is shown in panels (b) and (c), respectively

Thermometric measurements were performed to determine a numerical evaluation of the Fe_3O_4 nanoparticles heating efficiency. In particular, a sensitive digital thermometer was used to quantify the released heat using an AC magnetic field with f = 200, 300, and 400 kHz and field amplitude H_{AMF} between 200 and 400 Oe. For example, the heating-cooling transients for aqueous solutions containing Fe_3O_4 nanoparticles are demonstrated using liquid suspensions in a glass test tube enclosed in a Teflon holder. The temperature curves were produced when the MNPs were exposed to an AC magnetic field for 60 s at a frequency of 400 kHz and a peak amplitude of 300 Oe.

Fe_3O_4 nanoparticles aqueous suspensions of various concentrations (1, 3, 5, 10, 15, 25 mg/mL) were employed for the Fe_3O_4 nanoparticles after the magnetic solution was ultrasonicated for 15 minutes to preserve excellent stability and prevent nanoparticles agglomeration throughout the tests. Through MHT measurements, the specific loss power SLP was computed using the calorimetric approach. The calorimetric heat measuring procedures were performed using the Magnetic Hyper-Thermia MDK device. The heating response was tested within the range 50 and 400 Oe of magnetic field amplitude at f = 200, 300, and 400 kHz. The ΔT-t curves for Fe_3O_4 nanoparticles evaluated in a water medium with indicated colloidal suspension concentrations (H_AMF =400 Oe, f=400 kHz) is displayed in Fig. (7). The sample with a concentration of 5 mg/mL exhibits the highest temperature increase (ΔT ~6°C) in the low concentration regime, while the sample

with a concentration of 25 mg/mL exhibits the highest temperature increase (ΔT~17°C) in the higher concentration regime.

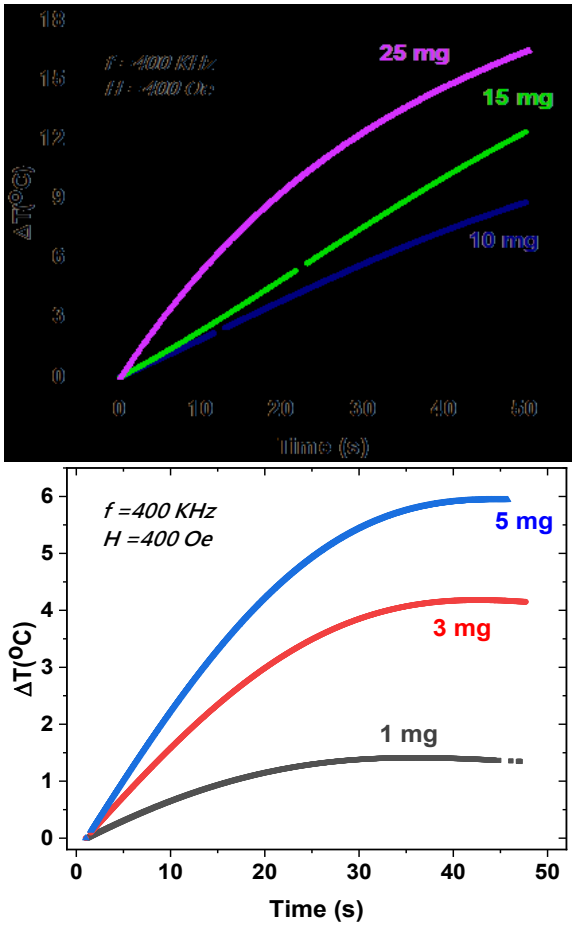

Fig. (7) Thermal response of Fe_3O_4 NPs tested in a water medium with various particle concentrations (the low concentration regime is shown in the top panel, and the high concentration regime is shown in the bottom panel) during maintaining constant magnetic field parameters at H_{AMF} =400 Oe and f=400 kHz

The heat dissipated in terms of SLP, given in W/g, was computed using the following formula [36-39]

$$SLP = C_S(\frac{\Delta T}{\Delta t})\frac{M_{Sol.}}{M_{MNPs}} \quad (7)$$

where C_s is the solvent specific heat capacity (C_{water}= 4.187 J/g.°C); M_{Sol} and M_{MNPs} are the masses of the solvent and MNPs used for measurement, and where $\Delta T/\Delta t$ is the temperature-time dependent starting slope of the heating curve

At a specific frequency (f=400 kHz), as shown in Fig. (8), SLP values rose in all sample cases when the applied magnetic field was increased from 50 to 400 Oe. However, for all samples, the applied field of 50 Oe produced the least increase in SLP values. In the results above, although there is a deviation from the linear response at higher frequencies (150-400 kHz), the field-amplitude-dependent SLP seemed to be linear at the lower frequency of (50-150 kHz). As a result, the SLP values exhibit the anticipated square dependence concerning the external field [40]. According to Alphandéry et al., the Fe_3O_4 nanoparticles corresponding SLP value increases nearly eightfold when the applied magnetic field intensity is nearly quadrupled. This suggests that SLP values should be measured under the same conditions as those used in magnetic hyperthermia therapy [41]. The performance of MNPs in converting applied electromagnetic energy into thermal energy is demonstrated in Fig. (9). Evidently, when f=400 kHz and H_{AMF} =400 Oe, the SLP value of all samples is maximized. It is remarkable that the concentration of exhibits the largest SLP values among others which might be due to oscillation behavior SLP dependence.

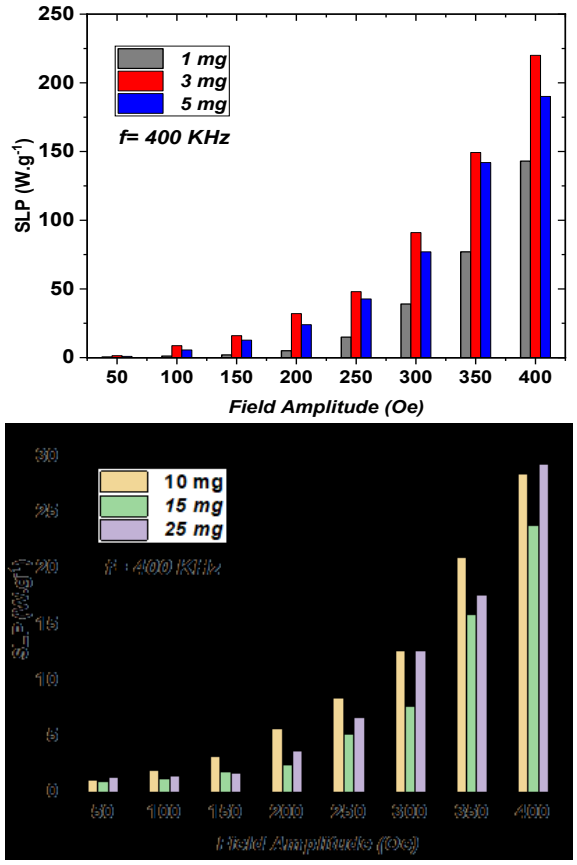

Fig. (8) The field-amplitude-dependent SLP for different Fe_3O_4 MNPs fluid concentrations measured at constant frequency f=400 kHz (top) represents the low concentration regime, (bottom) represents higher concentration regime

Measurements of hyperthermia were conducted using frequencies of 200, 300, and 400 kHz and constant applied magnetic fields that varied by 400 Oe in accordance with the biological safety criteria. The biological microenvironment can inhibit Brownian relaxation and has a major impact on the magnetic response of nanoparticles [42]. In order to verify the SLP concentration dependence with frequency, ferrofluids were used at varying concentrations, as depicted in Fig. (9). The typical pattern of all

measurements indicates that an increase in f results in a rise in the thermal response, which raises the SLP value. According to Soetaert et al., there is a linear relationship between SLP and AMF frequency, meaning that a higher SLP value is produced by an increase in f [43]. Remarkably, the SLP values displayed in Fig. (9) correspond to the samples' FESEM and DLS results, which support the idea that the size effect of Fe_3O_4 MNPs and magnetic properties influence the mechanisms of heat production. In addition, as depicted in Fig. (9), low concentration results revealed that SLP exhibited strong concentration-dependent oscillation behavior. Since there is no discernible dependence of SLP on the concentration of magnetic nanofuid hyperthermia, it is theoretically difficult to predict. But according to a number of recently published studies, it was unexpectedly found that the concentration of the nanofuid [44-50] affects the change in SLP. Given that this unexpected behavior may lead to a severely inaccurate prediction of the heat generation performance of nanofuid in clinical applications, this observation is not only scientifically intriguing but also medically significant. Based on these results, it was suggested that this phenomenon might be primarily caused by magnetic dipole interaction (MNPs) in nanofluids with varying inter-particle distances ($d_{(c-c)}$). Due to a chain-like arrangement of MNPs under AC magnetic fields, the strong magnetic dipole interaction, which is thought to be caused by a short inter-particle distance, may cause SLP to decrease [44,45,48].

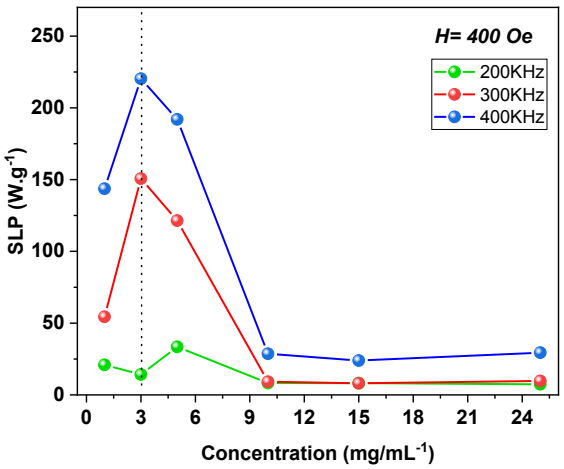

Fig. (9) Hyperthermia SLP measurements of constant maximum applied magnetic fields set at H_{AMF} =400 Oe and frequencies of 200, 300, and 400 kHz

4. Conclusions

In summary, Fe_3O_4 MNPs were prepared using the co-precipitation method. The MNPs with inverse spinel structure were confirmed of the pure magnetite with nearly spherical MNPs with mean size of ~42 nm. The hysteresis loop results demonstrated a significant low Hc value (3.1 Oe) with Ms of 38.73 emu/g. Additionally, the FORC analysis showed the presence of dipolar interaction. The ferrofluid containing Fe_3O_4 MNPs dispersed in distilled water medium at a concentration of 3 mg/mL produced the highest SLP value (220 W/g) and the highest temperature rise (ΔT~6 °C) for the sample with concentration 5 mg/mL. Due to a balanced combination of high Ms and low Hc with dipolar interactions the MNPs produced the maximum SLP. The ferrofluid with MNPs concentration at 25 mg/mL had the highest temperature rise (~16°C) and SLP value (~29.24 W/g). Our results of magnetic and calorimetric measurements on Fe_3O_4 nanoparticles highlights the key elements that contribute finding best heating efficiency with lower dosage and consequent toxicity which represents a challenge in using Fe_3O_4 nanoparticles for magnetic hyperthermia.

Acknowledgements

The authors would like to thank MDK Company's team and Department of Physics in the University of Kashan for their kind assistance.

References

[1] R.R. Shah et al., "Determining Iron Oxide Nanoparticle Heating Efficiency and Elucidating Local Nanoparticle Temperature for Application in Agarose Gel-Based Tumor Model", *Mater. Sci. Eng. C*, 68 (2016) 18-29.

[2] K. Wu et al., "Magnetic nanoparticles in nanomedicine: A review of recent advances", *Nanotech.*, 30(50) (2019) 502-518.

[3] A.E. Deatsch and B.A. Evans, "Heating Efficiency in Magnetic Nanoparticle Hyperthermia", *J. Magn. Magn. Mater.*, 354 (2014) 163-172.

[4] M. Kallumadil et al., "Suitability of commercial colloids for magnetic hyperthermia", *J. Magn. Magn. Mater.*, 321(10) (2009) 1509-1513.

[5] B. Thiesen and A. Jordan, "Clinical applications of magnetic nanoparticles for hyperthermia", *Int. J. Hyperth.*, 24(6) (2008) 467-474.

[6] C.L. Dennis and R. Ivkov, "Physics of heat generation using magnetic nanoparticles for hyperthermia", *Int. J. Hyperth.*, 29(8) (2013) 715-729.

[6] H.A. Albarqi et al., "Biocompatible Nanoclusters with High Heating Efficiency for Systemically Delivered Magnetic Hyperthermia", *ACS Nano*, 13(6) (2019) 6383-6395.

[7] E.L. Verde, "Field dependent transition to the non-linear regime in magnetic hyperthermia experiments: Comparison between maghemite, copper, zinc, nickel and cobalt ferrite nanoparticles of similar sizes", *AIP Adv.*, 2(3) (2012) 032120-032142.

[8] Y. Hadadian, A.P. Ramos and T.Z. Pavan, "Role of Zinc Substitution in Magnetic Hyperthermia

Properties of Magnetite Nanoparticles: Interplay between Intrinsic Properties and Dipolar Interactions", *Sci. Rep.*, 9(1) (2019) 18048.
[9] R. Otero-Lorenzo et al., "Solvothermally Driven Mn Doping and Clustering of Iron Oxide Nanoparticles for Heat Delivery Applications", *Chem. Eur. J*., 22(19) (2016) 6666-6675.
[10] R. Gupta and D. Sharma, "Manganese-Doped Magnetic Nanoclusters for Hyperthermia and Photothermal Glioblastoma Therapy", *ACS Appl. Nano Mater.*, 3(2) (2020) 2026-2037.
[11] P.M. Cardoso, G.J. de Moreno and S.G. Pachuca, "Effect of Cobalt Dopants on Magneto-Optic Conversion of Magnetite Nanostructures", *Iraqi J. Appl. Phys. Lett.*, 8(1) (2025) 25-28.
[12] S. Dutz and R. Hergt, "Magnetic nanoparticle heating and heat transfer on a microscale: Basic principles, realities and physical limitations of hyperthermia for tumour therapy", *Int. J. Hyperth*., 29(8) (2013) 790-800.
[13] M. Coïsson et al., "Hysteresis losses and specific absorption rate measurements in magnetic nanoparticles for hyperthermia applications", *Biochim. Biophys. Acta*, 1861(6) (2017) 1545-1558.
[14] J.-W. Kim et al., "Concentration-dependent oscillation of specific loss power in magnetic nanofluid hyperthermia", *Sci. Rep.,* 11(1) (2021) 733.
[15] C. Martinez-Boubeta et al., "Adjustable hyperthermia response of self-assembled ferromagnetic fe-MgO core-shell nanoparticles by tuning dipole-dipole interactions", *Adv. Func. Mater*., 22(17) (2012) 3737–3744.
[16] I. Andreu et al., "Same magnetic nanoparticles, different heating behavior: Influence of the arrangement and dispersive medium", *J. Magn. Magn. Mater*., 380 (2015) 341-346.
[17] D. Serantes, "Influence of dipolar interactions on hyperthermia properties of ferromagnetic particles", *J. Appl. Phys.,* 108 (2010) 073918.
[18] G.T. Landi, "Role of dipolar interaction in magnetic hyperthermia", *Phys. Rev. B,* 89 (2014) 014403.
[19] H.J. Mustafa, "Characterization and Comparison of Magnetite Nanoparticles Prepared by Coprecipitation and Autocombustion Techniques", *Iraqi J. Appl. Phys. Lett.*, 8(3) (2025) 885-88.
[18] A.F. Bakuzis et al., "Chain formation and aging process in biocompatible polydisperse ferrofluids: Experimental investigation and Monte Carlo simulations", *Adv. Coll. Interface Sci.,* 191-192 (2013) 1-21.
[19] S.P. Schwaminger et al., "Oxidation of magnetite nanoparticles: impact on surface and crystal properties", *Cryst. Eng. Commun.*, 19 (2017) 246.
[20] M.A. Dheyab et al., "Simple rapid stabilization method through citric acid modification for magnetite nanoparticles", *Sci. Rep.,* 10(1) (2020) 10793.
[21] R.D. Waldron, "Infrared Spectra of Ferrites", *Phys. Rev.*, 99 (1955) 1727-1735.
[22] A.K. Bordbar et al., "Characterization of Modified Magnetite Nanoparticles for Albumin Immobilization", *Biotech. Res. Int.*, 2014 (2014) 705068.
[23] Y. Sahoo et al., "Aqueous Ferrofluid of Magnetite Nanoparticles: Fluorescence Labeling and Magnetophoretic Control", *J. Phys. Chem. B*, 109 (2005) 3879-3885.
[24] S. Pathak et al., "Facile synthesis, static, and dynamic magnetic characteristics of varying size double-surfactant-coated mesoscopic magnetic nanoparticles dispersed stable aqueous magnetic fluids", *Nanomater.*, 11(11) (2021) 3009.
[25] A. Kumar and C. Kumar Dixit, "Advances in Nanomedicine for the Delivery of Therapeutic Nucleic Acids, Methods for characterization of nanoparticles", *Adv. Nanomed. Deliv. Therapeut. Nucleic Acids*, 12(1) (2017) 43-58.
[26] N.H. Yennawar et al., "Ch. 17 - A High-Throughput Biological Calorimetry Core: Steps to Startup, Run, and Maintain a Multiuser Facility", *Methods in Enzymology*, 567 (2016) 435-460.
[27] M.D. Nguyen et al., "Fe_3O_4 Nanoparticles: Structures, Synthesis, Magnetic Properties, Surface Functionalization, and Emerging Applications", *Sci*., 11(23) (2021).
[28] O.A. Hammadi, "Effects of Extraction Parameters on Particle Size of Iron Oxide Nanopowders Prepared by Physical Vapor Deposition Technique", *Iraqi J. Appl. Phys.,* 20(2B) (2024) 457-460.
[29] S. Ruta et al., "First order reversal curves and intrinsic parameter determination for magnetic materials; limitations of hysteron-based approaches in correlated systems", *Sci. Rep.,* 7 (2017) 45218.
[30] A.P. Roberts, C.R. Pike and K.L. Verosub, "First-order reversal curve diagrams: a new tool for characterizing the magnetic properties of natural samples", *J. Geophys. Res.*, 105 (2000) 28461-28475.
[31] C.R. Pike, A.P. Roberts and K.L. Verosub, "Characterizing interactions in fine magnetic particle systems using first order reversal curves", *J. Appl. Phys.*, 85 (1999) 6660-6667.
[32] D. Mayergoyz, "Mathematical models of hysteresis", *IEEE Trans. Magn.,* 22(5) (1986) 114-178.
[33] A.R. Muxworthy and D.J. Dunlop, "First-order reversal curve (FORC) diagrams for pseudo-

single-domain magnetites at high temperature", *Earth Planet. Sci. Lett.*, 203(1) (2002) 369-382.

[34] I. Andreu and E. Natividad, "Accuracy of available methods for quantifying the heat, power generation of nanoparticles for magnetic hyperthermia", *Int. J. Hyperth*., 29 (2013) 739–751.

[35] B. Kozissnik et al., "Magnetic fluid hyperthermia: Advances, challenges, and opportunity", *Int. J. Hyperth.,* 29 (2013) 706–714.

[36] S. Huang et al., "On the measurement technique for specific absorption rate of nanoparticles in an alternating electromagnetic field", *Meas. Sci. Technol*., 23 (2012) 035701.

[37] A. Jordan et al., "Magnetic fluid hyperthermia (MFH): cancer treatment with AC magnetic field induced excitation of biocompatible superparamagnetic nanoparticles", *J. Magn. Magn. Mater*., 201 (1999) 413-419.

[38] H. Gavilán et al., "How size, shape and assembly of magnetic nanoparticles give rise to different hyperthermia scenarios", *Nanoscale,* 13(37) (2021) 15631-15646.

[39] E. Alphandéry et al., "Heat Production by Bacterial Magnetosomes Exposed to an Oscillating Magnetic Field", *ACS Public. Collec.,* 115(1) (2010) 18–22.

[40] D. Soukup et al., "*in situ* measurement of magnetization relaxation of internalized nanoparticles in live cells", *ACS Nano*, 9(1) (2015) 231– 240.

[41] F. Soetaert et al., "Experimental estimation and analysis of variance of the measured loss power of magnetic nanoparticles", *Sci. Rep.,* 7(1) (2017) 6661.

[42] A. Wang et al., "Structural force arising from magnetic interactions in polydisperse ferrofuids", *Appl. Phys. Lett.,* 94(3) (2009) 212501.

[43] L.C. Branquinho et al., "Effect of magnetic dipolar interactions on nanoparticle heating efficiency: Implications for cancer hyperthermia", *Sci. Rep*., 3 (2013) 20–22.

[44] P. Ilg, "Equilibrium magnetization and magnetization relaxation of multicore magnetic nanoparticles", *Phys. Rev. B,* 95 (2017) 214427.

[45] S. Ota and Y. Takemura, "Characterization of Néel and Brownian relaxations isolated from complex dynamics influenced by dipole interactions in magnetic nanoparticles", *J. Phys. Chem. C,* 123 (2019) 28859–28866.

[46] D. Serantes et al., "Influence of dipolar interactions on hyperthermia properties of ferromagnetic particles", *J. Appl. Phys.,* 108 (2010) 073918.

[47] J.G. Ovejero et al., "Effects of inter- and intra-aggregate magnetic dipolar interactions on the magnetic heating efficiency of iron oxide nanoparticles", *Phys. Chem. Chem. Phys.,* 18 (2016) 10954-10963.

[48] I. Conde-Leboran et al., "A single picture explains diversity of hyperthermia response of magnetic nanoparticles*", J. Phys. Chem. C,* 119 (2015) 15698-15706.

